Sub-Wavelength Waveguide Michelson Interferometer Sensors

Asela Perera[a], Jianhao Shen, Swapnajit Chakravarty[b]
Department of Electro-Optics and Photonics, University of Dayton, OH, USA 45469

ABSTRACT

We experimentally demonstrate an asymmetric Michelson interferometer sensor with subwavelength waveguides in a silicon-on-insulator (SOI) platform with experimentally demonstrated bulk sensitivity ~775nm/RIU. Numerical simulations indicate feasibility to achieve high sensitivity ~70,000nm/RIU in optimized device geometries.

Keywords: Michelson Interferometer, subwavelength waveguide, silicon photonics

1. INTRODUCTION

Evanescent field silicon photonics in a silicon-on-insulator or silicon-nitride-on-insulator platforms have been effectively utilized to demonstrate chemical and biosensors over the past decade with applications in the detection of nucleic acids and protein biomarkers for cancers, viruses and infectious diseases, and environmental toxins. By balancing the requirements for efficient low-loss transmission through the waveguide and enhancing light-matter interaction such as with molecules binding on the high index material surfaces in resonant microcavities, slow light and interferometer geometries, various high sensitivity biosensors have been experimentally demonstrated down to few femtograms/ml. various slotted microcavities and waveguides have been experimentally demonstrated. In recent years, subwavelength waveguides [1-2] have demonstrated high bulk spectral sensitivities approaching ~500nm/RIU (RIU=refractive index unit) in periodic structures with lattice constant (Λ) <<($\lambda/2n_{eff}$) where n_{eff} is the effective index at wavelength λ. [3-5] While most experimental demonstrations have been in subwavelength ring resonator geometries, in this research, in addition to experimental demonstration of bulk spectral sensitivity ~775nm/RIU in subwavelength waveguides in interferometer configurations, we investigate optimized geometries that can reach sensitivities ~70,000nm/RIU in compact dimensions. In contrast to Mach-Zehnder interferometer (MZI) sensors of the same geometric interferometer arm lengths, the reflected path in Michelson interferometers (MI) doubles the optical path length, and thus effectively doubles the phase shift in the presence of an analyte [6]. The interference fringe linewidths are narrowed compared to the equivalent MZI and would thus enable smaller changes in analyte concentration to be discerned from the fringe spectra.

2. DESIGN AND EXPERIMENT

Fig. 1(a) shows a schematic of the Michelson Interferometer (MI) chem-bio analyte sensor formed with subwavelength waveguides. Fig. 1(b) shows a top view microscope image of the fabricated Michelson interferometer (MI) sensor device with subwavelength waveguides. Subwavelength waveguides (SWGs) with different lengths 50μm and 200μm are fabricated on the reference arm and the signal arm respectively. Fig. 1(c) shows the scanning electron microscope (SEM) image of the subwavelength waveguide along with the tapering geometry used to gradually taper the SWG section from the access strip waveguide section. The reference arm is covered with silicon dioxide top cladding, while the SWG on the signal arm is exposed to the analyte by etching away the top oxide cladding down to the BOX layer. Fig. 1(d) and (e) show the transmission spectrum and the electric field intensity profile of in-house designed 2×2 MMIs that are used to split and then combine the two arms of the interferometer. A waveguide loop mirror connects the two output arms and reflects the light back to the interferometer arms thereby doubling the interaction length compared to an equivalent Mach-Zehnder interferometer with the same geometric interferometer arm lengths.

Initial simulations were performed to determine the SWG dimensions that would achieve large shifts in the interference fringes in the targeted wavelength range between 1540nm and 1560nm where the foundry fabricated grating couplers had the peak transmission. Figs. 2(a) and 2(b) show the variation in SWG effective index and group index respectively as a function of wavelength for a representative liquid, acetone (refractive index n=1.3586). In Fig. 2(c), the bulk spectral

a pereraa2@udayton.edu;
b schakravarty1@udayton.edu; phone 1 937 229-2747;

Frontiers in Biological Detection: From Nanosensors to Systems XVI, edited by Amos Danielli, Benjamin L. Miller, Sharon M. Weiss, Proc. of SPIE Vol. 12861, 1286106
 · 1605-7422 · doi: 10.1117/12.3003051

sensitivity of the asymmetric SWG MI is seen to increase with increasing lattice constant (period) as the dispersion curve and hence the photonic band edge of the periodic structure gradually red shifts into the wavelength range of interest.

Fig. 3(a) plots the simulated transmission spectrum measured with analyte acetone (n=1.3586) and a hypothetical liquid with refractive index n=1.3596 (Δn=0.001) with the asymmetric SWG MI in Fig. 1. The experimental bulk sensitivity is estimated at 775nm/RIU from Fig. 3(b) by monitoring the interference fringe shift in acetone and ethanol (n=1.3614), close to the simulated 780nm/RIU. With the same device length as in Fig. 1, the interferometer arm lengths were further optimized and simulations indicate a bulk sensitivity of ~70,000nm/RIU. Given the wide fringe linewidth, such high bulk sensitivity is particularly important when monitoring for extremely small changes in the refractive index as is typical with low concentrations of biomarkers in biosensing experiments. Further simulations and measurements are in progress.

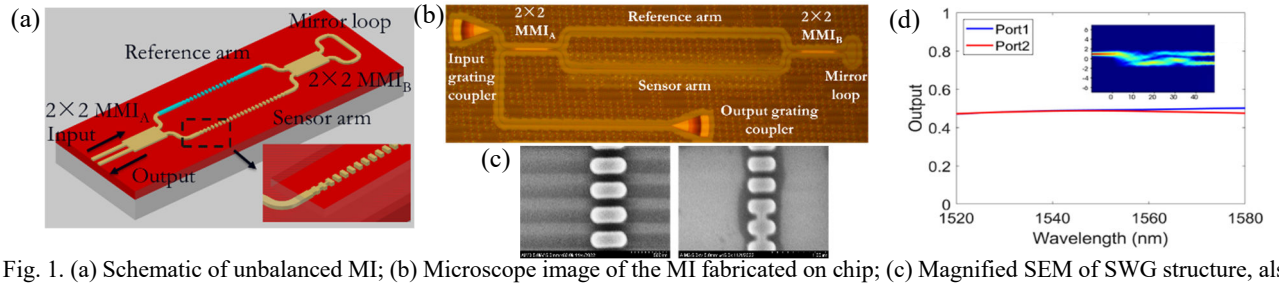

Fig. 1. (a) Schematic of unbalanced MI; (b) Microscope image of the MI fabricated on chip; (c) Magnified SEM of SWG structure, also showing section of adiabatic taper coupler; (d) Transmission spectrum and electric field intensity profile of 2×2 MMI in inset.

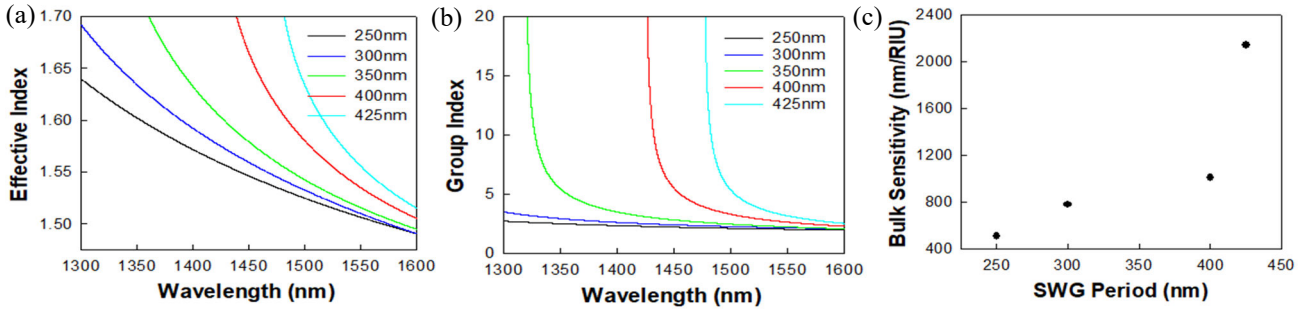

Fig.2. (a) Effective index (b) Group Index versus wavelength for different SWG pitch. (c) Variation of bulk spectral sensitivity versus lattice constant.

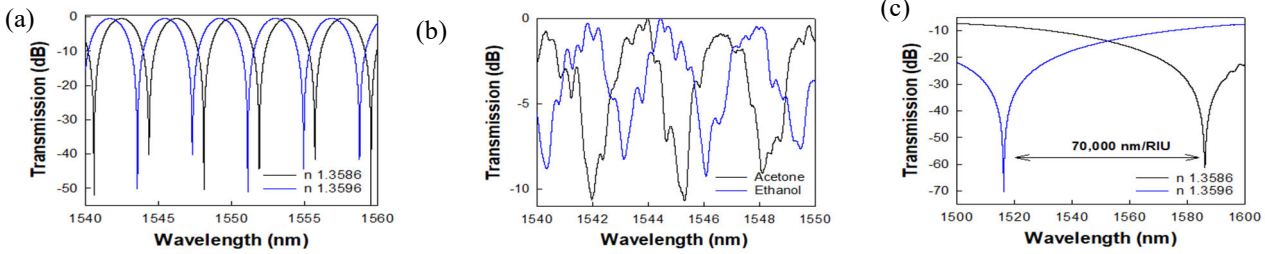

Fig.3. (a) Simulated and (b) experimental shift of interference fringes for SWG pitch Λ=300nm. (c) Optimized device geometry at Λ-300nm with simulated spectral sensitivity 70,000nm/RIU for same interferometer arm length.

After chemical sensing experiment, bio sensing experiments were performed by detecting conjugate bindings of biotin-streptavidin. First, oxygen plasma treatment was done to create OH bonds on chip Si devices as depicted in Fig 4. Next, a silane layer was grown on Si devices using APTES (amino-propyl tri-ethoxy silane) to immobilize receptor biomolecules. Glutaraldehyde treatment was done to attach aldehyde group. Biotin was next dispensed on the chip as a primary antibody and bovine serum albumin (BSA) was dispensed to remove all other non-specific bindings. Finally, different concentrations of streptavidin (0.1 ng/ml-1000ng/ml) were dispensed on the chip.

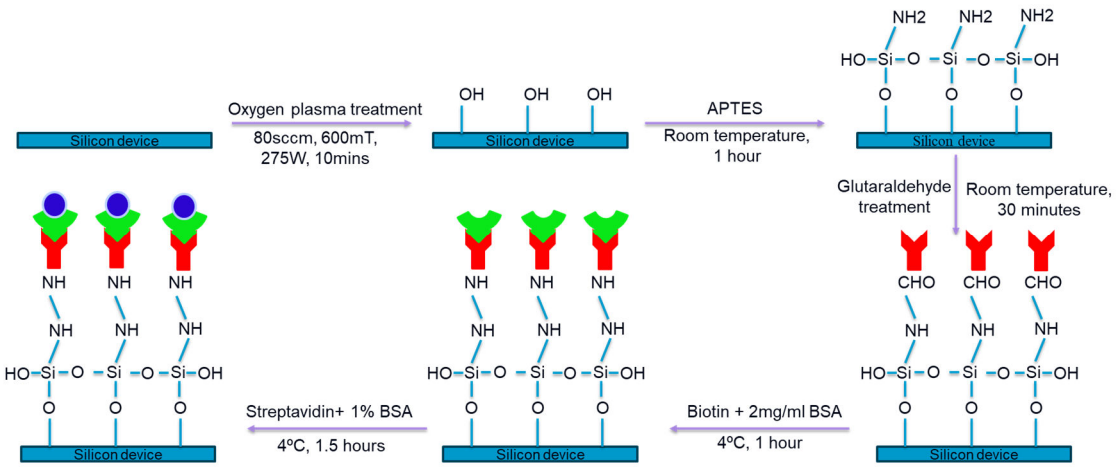

Fig 4. Procedure to get different concentrations of biotin-streptavidin conjugate bindings on Si devices.

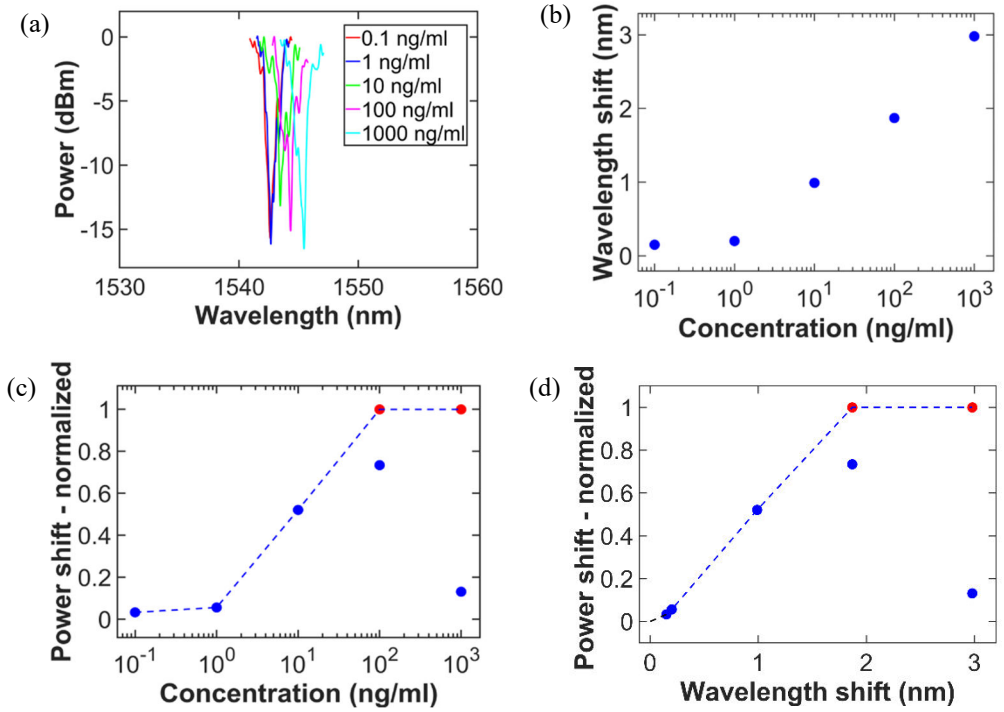

Fig. 5. (a) Power versus wavelength graph for different concentrations of streptavidin (b) Wavelength shift versus concertation (c) Power shift - normalized versus concentration (d) Power shift - normalized versus wavelength shift.

As in Fig. 5(a) for different concentrations of streptavidin, the interference fringes red shifted. The maximum shift was obtained for 1000 ng/ml sample, and it was recorded as 2.9 nm. Wavelength shift increases with increasing concentration of streptavidin as shown in Fig. 5(b). In order to measure wavelength shifts, a tunable laser source is needed. However, it tunable laser sources are very expensive. Instead of measuring wavelength shift ($\Delta\lambda$), power shift(ΔP) can be measured for fixed wavelength as in Fig. 5(c) by a photodetector. Here, ΔP is expected to increase with increasing concentrations. The decrease in DP at higher concentrations arises from the limited FSR resulting the overlapping of the adjacent fringes with the fixed wavelength at which the intensity is measured. If the free spectral range is high, power shift at those last two concentrations would reach the highest power shift shown in red dots. To avoid this problem, device length should

decrease so that free spectral range can be increased. However, simulations show that reducing the signal arm length results in a simultaneous decrease in the phase sensitivity. Power shift versus wavelength shift is depicted in Fig 5(d).

Limit of detection (LOD) calculations were done to validate performance of the device. Phase sensitivity was calculated by using following formular as 7.3 rad/ RIU. μm.

$$\text{Phase sensitivity} = \frac{\text{bulk sensisity}}{\text{free spectral range}} \times \frac{2\pi}{\text{length of the sensing arm}}$$

$$= \frac{775\ \text{nm/RIU}}{3.35\ \text{nm}} \times \frac{2\pi}{200\ \mu\text{m}} = 7.3\,\frac{\text{rad}}{\text{RIU. }\mu\text{m}}$$

$$\text{Limit of Detection (LOD)} = \frac{\text{minimum phase detection}}{\text{phase sensitivity} \times \text{length of the sensing arm}}$$

For a system which has detectable minimum fringe wavelength shift using a tunable laser source (or broadband source) as 20pm or 1pm, LOD is estimated as 2.6×10^{-5} RIU and 1.3×10^{-6} RIU respectively. Instead of wavelength shift, LOD can be obtained by measuring power shift. Our sensing system can be considered to be amplitude noise limited since fringe Q is low (~1000). In our measurement setup, laser intensity fluctuation is less than 100nW. Typical dark current in waveguide integrated photodetectors is 10nA (~ 10nW for responsivity 1A/W). By considering all sources of noise in our measurement, the minimum detectable signal power due to a sensing event can be conservatively estimated as 100nW. With a system that has minimum detection signal as 100 nW a fixed wavelength laser can achieve LOD as 1.1×10^{-6} RIU. We designed devices that achieve very high 30,000 nm/RIU when measuring the wavelength shift in the interference fringes. Higher bulk sensitivities 70,000nm/RIU were also achieved by adjusting the reference arm length based on the ratio of propagating group indices in the two interferometer arms, while keeping the signal arm fixed. However, the simulated phase sensitivity and the LOD values do not change from the simulated SWWG values of the same signal arm length since the FSR of such a device very high~29nm (for the case of bulk sensitivity 30,000nm/RIU).

3. CONCLUSIONS

Experimentally demonstrated reflected path enhanced SWG Michelson Interferometer for chemical sensing and bio sensing. Phase sensitivity is recorded as 72,678 rad/RIU. cm. By monitoring intensity changes in interferometers, our device can potentially reach a limit of detection of 1.1×10^{-6} RIU.

4. ACKNOWLEDGEMENT

This work is supported by the National Science Foundation (NSF) under grant #2210707 and #2315085. A.P acknowledges the University of Dayton graduate summer fellowship and SPIE travel grant. Fabrication was supported by AIM Photonics.

5. REFERENCES

[1] P. J. Bock, P. Cheben, J. H. Schmid, J. Lapointe, A. Delâge, S. Janz, G. C. Aers, D. Xu, A. Densmore, and Trevor J. Hall, Opt. Express 18, 20251 (2010)
[2] P. Cheben, R. Halir, J.H. Schmid, H. A. Atwater, D. R. Smith. Nature 560, 565 (2018)
[3] J. Flueckiger, S. Schmidt, V. Donzella, A. Sherwali, D. M. Ratner, L. Chrostowski, K. C. Cheung, Opt. Exp. 24 (14), 15672 (2016).
[4] L. Huang, H. Yan, X. Xu, S. Chakravarty, N. Tang, H. Tian, R. T. Chen, Opt. Exp. 25 (9), 10527 (2017).
[5] H. Yan, L. J. Huang, X. Xu, S. Chakravarty, H. P. Tian, R. T. Chen, Opt. Exp. 24 (26), 29725 (2016).
[6] J. Shen, D. Donnelly, S. Chakravarty, Proc. of the SPIE 12532, 125320R (2023).